sustainability

MDPI

Article

Effect of Teflon-Coated PVDF Membrane on the Performance of a Solar-Powered Direct Contact Membrane Distillation System

Pon Pavithiran C. K. [1], Govindaraj Kumaresan [2,*], Raju Abraham [3], Ravichandran Santosh [4,5] and Ramalingam Velraj [2]

1 Department of Mechanical Engineering, Vellore Institute of Technology, Vellore 632014, India; ponpavithiranck@gmail.com
2 Institute for Energy Studies, CEG Campus, Anna University, Chennai 600025, India; velrajr@gmail.com
3 National Institute of Ocean Technology, Chennai 600025, India; abraham@niot.res.in
4 Energy and Environmental Engineering Laboratory, Department of Mechanical Engineering, Hanyang University, 55 Hanyangdaehak-ro, Sangnok-gu, Ansan 15588, Gyeonggi-do, Korea; santoshravi90@gmail.com
5 ERICA Industry-University Cooperation Foundation, Hanyang University, 55 Hanyangdaehak-ro, Sangnok-gu, Ansan 15588, Gyeonggi-do, Korea
* Correspondence: gkumaresan75@gmail.com

Abstract: The present study dealt with the generation of freshwater through the direct contact membrane distillation (DCMD) technique, powered by an evacuated tube solar collector (ETSC). The major objective of the present work was to determine the optimum conditions of fluid flow rate and temperature for maximum freshwater productivity across both the feed and permeate sides of the membrane module. A flat hydrophobic membrane composed of polyvinylidene fluoride (PVDF) coated with Teflon was utilized for the DCMD process. The rate of freshwater production was examined with the variation in the feed/permeate flow rates (from 3 to 7 LPM) and feed temperature (from 45 °C to 75 °C) for a constant permeate-side temperature of 30 °C. The experimental results indicated that a maximum freshwater productivity of 45.18 kg/m^{2}h was achievable from the proposed system during its operation with a high solar heated inlet feed temperature of 75 °C and mass flow rates of 7 LPM across both sides of the membrane. Further, a detailed assessment of the performance parameters indicated that the present solar-powered DCMD system exhibited a maximum evaporative efficiency of about 80% and temperature polarization coefficient (TPC) of 0.62 respectively.

Keywords: direct contact membrane distillation; flux production; freshwater; Teflon-coated PVDF membrane; temperature polarization coefficient

check for updates

Citation: C. K., P.P.; Kumaresan, G.; Abraham, R.; Santosh, R.; Velraj, R. Effect of Teflon-Coated PVDF Membrane on the Performance of a Solar-Powered Direct Contact Membrane Distillation System. *Sustainability* **2022**, *14*, 6895. https://doi.org/10.3390/su14116895

Academic Editor: Agostina Chiavola

Received: 29 April 2022
Accepted: 3 June 2022
Published: 5 June 2022

1. Introduction

The rapid growth of the worldwide population has led to a tremendous increase in the global demand for freshwater, a fast-depleting finite natural resource that is vital to life on earth. Based on a real-time statistical analysis by the World Resources Institute, it has been forecasted that by the year 2040, the demise of about 3.5 million people would be attributed to insufficient water supply and lack of sanitation [1]. The United Nations World Water Development Report signifies that, presently, around 3.7 billion people in the world face water scarcity issues and it may increase to ~5.6 billion by the year 2050 [2]. This issue of freshwater scarcity can be addressed by the adoption of water purification methods such as desalination technology. Among the two major distinct methods of desalination, nearly 50% of water purification is achieved through pressure-driven membrane techniques and the remaining is via thermal-driven purification techniques [3]. However, owing to the reduction in system efficiency due to membrane fouling, nonmembrane thermal-based purification methods are widely adopted in Gulf countries [4]. To minimize the membrane fouling issues, an effective method of membrane distillation (MD) is adopted [5].

MD is a relatively efficient technology that combines the advantages of both thermal and membrane desalination [6]. This method can be subdivided into direct contact, vacuum-based, sweeping gas, and air gap technologies. Comparatively, direct contact membrane distillation (DCMD) is regarded as one of the most efficient methods of desalination among the aforementioned technologies owing to its advantages of lower conductive heat loss and resistance between the hot and cold solutions [7]. Several research works have been attempted to improve the performance of the DCMD system. Yang et al. experimentally investigated the performance of a DCMD module under fixed feed- and cold-side temperatures of 70 °C and 25 °C, respectively [8]. The authors identified that a maximum permeate flux of 68 kg/m^2h was achieved by the DCMD module owing to the significant difference in the volatility and vapor pressure across the feed and cold sides.

In general, the temperature gradient functions as a driving factor for the transfer of evaporated vapor from the feed to the permeate side through a thin hydrophobic membrane [9]. Therefore, structural and material variations in the membranes used can help in improving the DCMD system's performance. Bodell attempted to utilize a silicon rubber hydrophobic membrane considering its high resistance to membrane fouling [10]. Results indicated that the freshwater was efficiently extractable from the contaminated brine and sewage water, with the use of the above silicon-based membrane with minimum energy consumption. Similarly, Wu successfully modified the hydrophilic membrane into a hydrophobic nature through radiation grafting and plasma polymerization processes that contributed to achieving a 99.1% sodium chloride rejection rate [11]. Kong et al. attempted a similar modification to the membrane's hydrophilic to hydrophobic nature through the octofluorocyclobutane polymerization process and the results indicated that the membrane exhibited a ~92.1% retention coefficient during the production of freshwater [12]. Unlike the surface modification over the hydrophilic membrane to achieve hydrophobicity, it has been identified that hydrophobic membranes can be directly utilized in MD systems efficiently. However, the effect of higher variable temperature and pH concentration of the solution affects the membrane's hydrophobic nature, hindering its efficiency and continuous adoption for the MD process [13]. Therefore, the hydrophobic membranes are designed in such a manner that the vapor pressure passing through the membrane surface is less than the liquid entry pressure (LEP) that can be determined using the Young–Laplace equation [14,15]. This LEP represents the minimum hydrostatic pressure that aids in the passage of liquid across the membrane [16]. A lower value on LEP restricts the liquid flow and enables efficient passage of vapor through the membrane, resulting in higher freshwater production. Therefore, considering the above advantages of the hydrophobic membranes, they have been widely adopted and tested in DCMD modules consisting of materials such as polyvinylidene fluoride (PVDF), polytetrafluoroethylene (PTFE) [17], polypropylene, and polyethylene (PE). However, among the above configurations, PVDF has been identified to exhibit superior properties that include high mechanical rigidity, thermal stability, chemical resistance, and high hydrophobicity, which collectively play a major role in the performance improvement of the DCMD system [18]. Thus, several researchers have experimented with both the PVDF standalone membrane [19] and PVDF blended with other specific materials such as halloysite (HNT) [20], hexafluoropropylene (HFP) [21], and multiceramics [22]. The investigations with the incorporation of the above hybrid membranes were carried out with either conventional or nonconventional sources of energy. Hence, the DCMD system can also be operated with nonconventional sources of energy such as solar [23], geothermal [24], and industrial waste heat [25], which makes it an energy-saving and environmentally friendly MD technology.

Owing to the predominant availability of solar energy, it is potentially used to heat the feed-side fluid for achieving the desired temperature range [11]. The heating process is accomplished using an efficient solar collector such as a flat plate collector, evacuated tube collector (ETC), compound parabolic collector (CPC), solar pond, or even a solar still [26,27]. Chandrashekara et al. compiled a comprehensive list of all the thermal desalination technologies powered by solar energy [28]. The reported literature indicates that the use of solar energy in the MD process contributes to the cost-effective production of freshwater. Utilization of solar energy for the DCMD process generally generates a flux output in the range of 0–6 L/m^{2}h, and the variation in the flux chiefly depends on the factors such as the drop in temperature across the membrane, the salinity of water, and the lower hot temperature [29]. Hogan et al. designed a computer simulation process of the solar-powered water desalination plant for domestic use with a capacity of 50 kg/day to predict the system's behavior under various parametric conditions. It was identified that the system efficiently worked under the optimized conditions of the required solar collector area of 3 m^2 along with the 1.8 m^2 membrane [30].

Thus, from the present perspective, it can be identified that solar energy can be efficiently utilized for the energy-efficient operation of the DCMD process, and increasing the hydrophobic nature of the membrane contributes to an increment in the process efficiency, leading to improved freshwater production. Considering the above characteristics, the current experimental study aims to investigate the performance of a solar-powered DCMD distillation system with an inbuilt PVDF membrane coated with Teflon, to improve the hydrophobic nature of the commercial PVDF membrane. The present work also focuses on evaluating and achieving a maximum membrane flux for the selected varying conditions of feed and permeate flow rates, along with the identification of optimum flow characteristics for maximum freshwater productivity. A detailed experimentation was carried out by increasing the temperature of the feed side from 45 °C to 75 °C using a solar ETC and maintaining a constant permeate-side temperature of 30 °C. Further, the performance assessment factors such as evaporative efficiency, temperature polarization coefficient (TPC), and optimal flow rate on either side of the selected membrane are evaluated. Thus, the major objective of the present work was to evaluate the effect of utilizing a Teflon-coated PVDF membrane in the solar-powered DCMD process and to determine the optimum operational conditions across the feed and permeate sides for achieving maximum permeate flux that contributes to maximum freshwater productivity. The following section describes the experimental methodology along with the instrumentation and various performance evaluation factors considered for evaluating the performance of the solar ETC-powered DCMD system. Subsequently, the major results achieved from the present work highlighting the feasibility of utilizing a Teflon-coated PVDF hydrophobic membrane on the DCMD module are discussed in detail under the "results and discussion" section with comparison of the present work with similar literature. This is followed by the uncertainty and a detailed cost analysis to evaluate the economic feasibility of the present system. Finally, the major findings from the present study are summarized under the conclusion section.

2. Experimentation

2.1. Experimental Methodology

The schematic layout of the solar-powered DCMD system utilized in the present study is shown in Figure 1. The experimentation was carried out using a solar ETC-powered DCMD test setup fabricated and erected (Figure 2) at the National Institute of Ocean Technology (NIOT), Chennai city, India (12.97° N latitude, 80.04° E longitude), where the favorable solar conditions for water heating exists. Figure 2a depicts the major experimental components that include a laboratory-scale DCMD module, differential pressure transducers, flow meter, and data acquisition system (DAQ) for constant recording and monitoring of the data during experimentation. The DCMD module consisted of sixteen modules arranged one after another to produce an effective contact area of 1 m^2. The sectional area of the Teflon-coated hydrophobic membrane was 250 mm × 250 mm, made of PVDF material. The experimentation involved the usage of saline water. Therefore, the modules and freshwater recirculation unit were fabricated using corrosion-resistant stainless-steel material of grade 316 and polypropylene. During experimentation, a fixed cold-side permeate temperature of 30 °C was maintained with a variation in the hot-side feed temperature for 45 °C to 75 °C, with the assistance of a solar ETC.

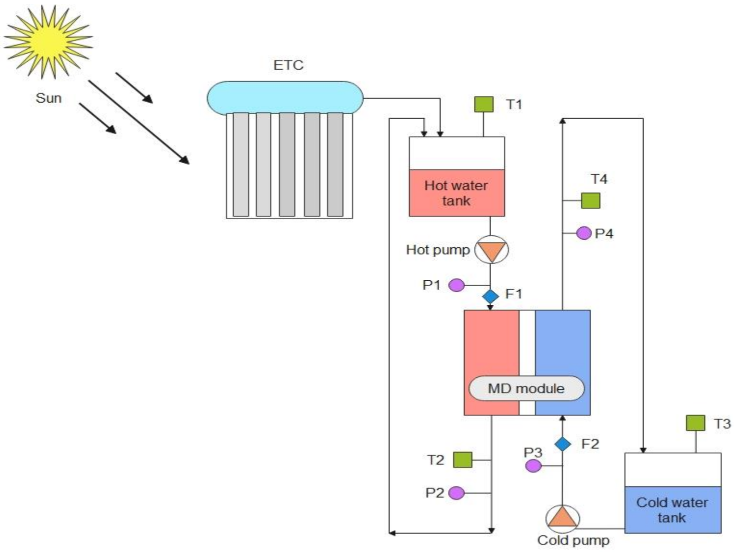

Figure 1. Process flow diagram of solar ETC-powered DCMD system.

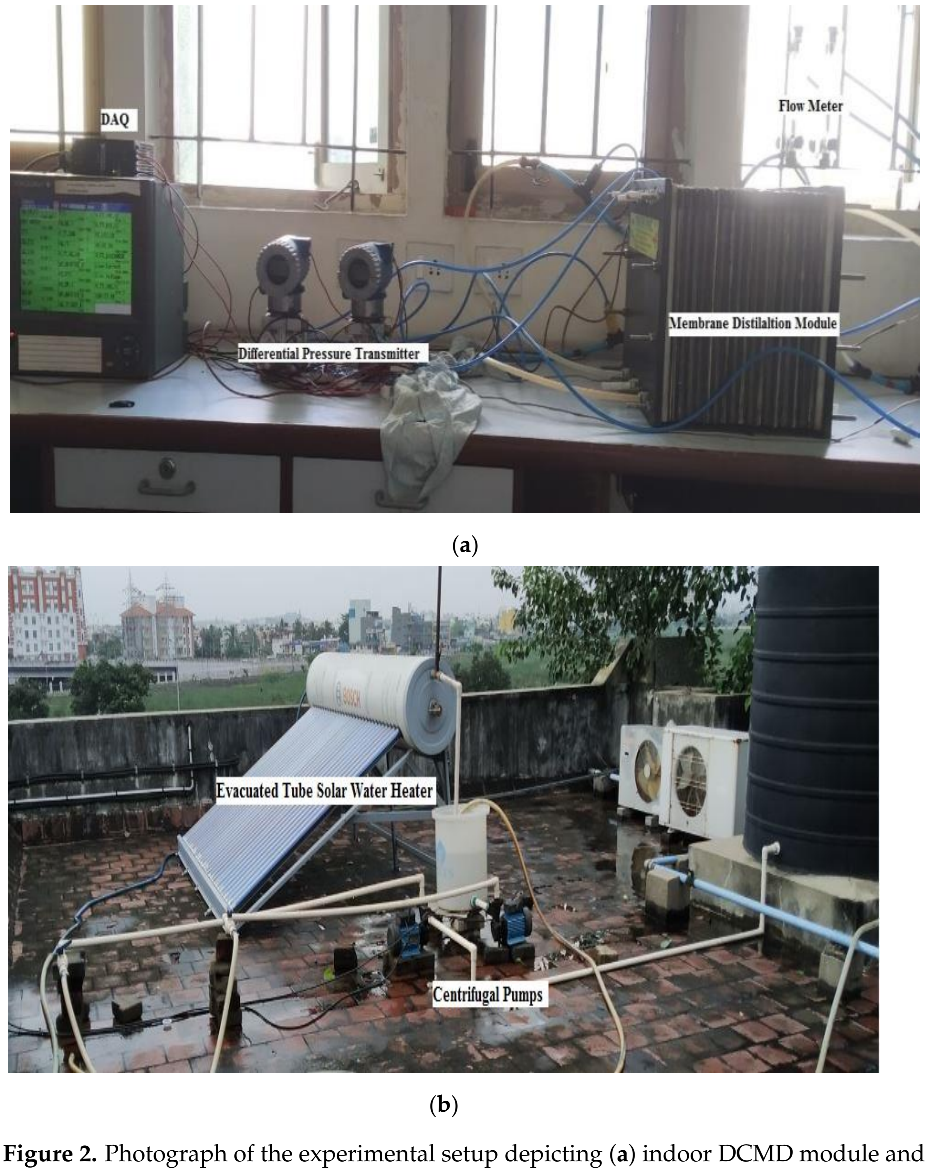

Figure 2. Photograph of the experimental setup depicting (**a**) indoor DCMD module and (**b**) outdoor solar ETC with auxiliary connections.

The feed solution was the groundwater collected at NIOT, Chennai, which is located at a distance of 10 km from the shore. The collected feed solution was stored in a separate feed water tank from which it was directed to the solar ETC of 300 L/day capacity. The specified solar ETC consisted of 20 evacuated tubes of 58 mm outer diameter and 1800 mm length, selected based on its large storage capacity that can be operated under fluctuating solar conditions. Prior to the entry of the feed water into the solar ETSC, it was subjected to a simple filtration procedure to remove any solid particles present in it. The hot feed solution from the exit of the solar ETC was stored in an insulated storage tank of 50 L capacity. Subsequently, the hot water from the insulated tank was made to flow across the feed side of the membrane in the DCMD module and the cold freshwater was allowed to flow across the other permeate side of the membrane. The hot and cold fluid mass flow rates were varied with the values of 3, 5, and 7 L/min (LPM). The hydrophobic Teflon-coated PVDF membrane permitted the penetration of the evaporated vapor by filtering the residues across the hot side. Subsequently, the vapor on reaching and coming into contact with the permeate-side fluid condensed to generate freshwater that was finally collected in the freshwater tank, and the production rate increased over repetitive cycles.

2.2. Measurement and Instrumentation

During experimentation, the key performance indicators were measured to evaluate the performance of the solar ETC-powered DCMD system. These parameters included the inlet (T_{hi}) and outlet (T_{ho}) temperatures of the feed across the feed side, pressure difference (d_{Ph}) across the hot side of the hydrophobic membrane, inlet (T_{ci}) and outlet (T_{co}) temperatures of the cold-side fluid, and pressure difference (d_{Pc}) across the permeate side. The temperature at various locations was measured using Pt100 RTD sensors (accuracy of ± 0.2 °C), and pressure transmitter sensors (Invensys Foxboro, accuracy of 1.0%) were utilized to measure the pressure difference characteristics. All the sensors were calibrated before usage and were connected to a DAQ (Yokogawa make, DX220-1-2) for constant monitoring and storing the measured data at a regular time interval of 2 s (Figure 2a). The feed and the freshwater flow across the DCMD module were regulated using respective water pumps (hot pump and cold pump) of a capacity of 0.745 kW each. The hot and cold fluid flow rates were monitored using respective rotameters (F1 and F2, Figure 1) and they were regulated using individual ball valves.

2.3. Performance Assessment

The various performance indices considered for evaluating the performance of the solar ETC-powered DCMD system are discussed in this section.

2.3.1. Permeate Mass Flux

The vapor flux that penetrates through the membrane is dependent on the difference in the vapor pressure of water on the feed and permeate sides, which can be utilized to predict the amount of distillate rate generated across the cold side. The mass flux of the permeate can be determined as:

$$J_w = B_m(P_{wf} - P_{wp}) \tag{1}$$

where J_w represents the permeate flux (kg/m^{2}s). P_{wf} and P_{wp} are the vapor pressure (Pa) across the feed side and permeate sides, respectively. Further, B_m represents the mass transfer coefficient, which can be calculated based on the Knudsen number as follows.

$$k_n = \frac{\lambda}{d_p} \tag{2}$$

where λ represents the mean free path of the vapor molecules transported through the membrane pore of size "d_p".

2.3.2. Vapor Pressure of Feed and Permeate

The vapor pressure on both sides of the membrane's surface was calculated from the Antoine equation with varying membrane temperature across the feed (T_{mf}) and permeate sides (T_{mp}) [31]. Using these temperatures, the vapor pressure in Equation (1) was calculated based on Equations (3) and (4).

$$P_{wf} = \exp(23.1964 - \frac{3816.44}{T_{mf} - 46.13}) \quad (3)$$

$$P_{wp} = \exp(23.1964 - \frac{3816.44}{T_{mp} - 46.13}) \quad (4)$$

where P_{wf} and P_{wp} are the vapor pressure (Pa) across the feed side and permeate sides, respectively.

2.3.3. Temperature Polarization Coefficient (TPC)

As the TPC cannot be measured directly, it can be determined using the hydrodynamic conditions across both sides of the Teflon-coated PVDF membrane. The temperature difference between the evaporation and condensation membrane surfaces was compared to the temperature difference between the feed and permeate streams to determine the *TPC* as follows [31]:

$$TPC = \frac{T_{fm} - T_{pm}}{T_f - T_p} \quad (5)$$

where T_{fm}, T_{pm}, T_f, and T_p represent the feed-side membrane temperature, permeate-side membrane temperature, bulk feed temperature, and bulk permeate temperature, respectively.

2.3.4. Evaporative Efficiency of the System (EE)

The evaporative efficiency (or) thermal efficiency parameter characteristics of the MD process are defined by the ratio of the heat required (Q_V) for evaporation to the total heat input (Q_V + Q_C) to the membrane module, which is always lower than unity. It is expressed as:

$$EE = \frac{Q_V}{Q_V + Q_C} \quad (6)$$

In the above equation, Q_V and Q_C were calculated using Equations (7) and (8), respectively.

$$Q_V = J_W \times \Delta H \quad (7)$$

$$Q_C = (\frac{K_m}{\partial}) \times (T_{mf} - T_{mp}) \quad (8)$$

where Q_V represents the heat transfer of the membrane through its pores by the evaporative mass flux (W/m^2), Q_C is the heat transfer through the membrane by the process of conduction (W/m^2), and ΔH represents the enthalpy of evaporation (kJ/kg).

3. Results and Discussion

A series of experiments were conducted to evaluate the viability of utilizing the solar ETC for the DCMD process to convert groundwater into freshwater. The feasibility of utilizing the Teflon-coated PVDF hydrophobic membrane on the performance of the DCMD module was assessed along with the process of optimizing the process parameters to identify the reliable flow condition across the feed and permeate sides for maximum freshwater productivity.

3.1. Effect of Feed Temperature on Permeate Flux for Varying Feed/Permeate Flow Rate

Different combinations of feed (m_f) and permeate (m_p) flow rates (3, 5, and 7 LPM) were considered to evaluate their combined effect on the variation in the membrane's permeate flux characteristics. Figure 3 shows the variation in the permeate flux with respect to varying feed temperatures (45 to 75 °C) for the three different mass flow rates maintained across both sides of the membrane in the DCMD module. The figure indicates that the permeate flux increased significantly at a higher feed temperature (75 °C) and a maximum flow rate of 7 LPM was achieved for both feed and permeate solutions. This can be attributed to the higher vapor pressure gradient experienced across the membrane for the above combinations of feed temperature and fluid flow rates, which contributes to the maximum driving potential for higher flux production [32]. It can be identified that a similar increasing trend of permeate flux existed for all the flow rates considered with an increase in the feed-side temperature. A maximum flux of 45.18 kg/m^{2}h was achieved when the mass flow rate on both sides of the membrane was maintained at 7 LPM, with feed and permeate inlet temperatures of 75 °C and 30 °C, respectively. However, when the flow rate was minimum (3 LPM) on both sides of the Teflon-coated PVDF membrane, the flux production reduced to 5.19 kg/m^{2}h (Figure 3). This can be attributed to the lower heat transfer coefficient potential experienced across the surface of the membrane owing to the decreasing Reynolds and Nusselt numbers, achieved as a consequent result of lower flow rates of feed and permeate solutions [33].

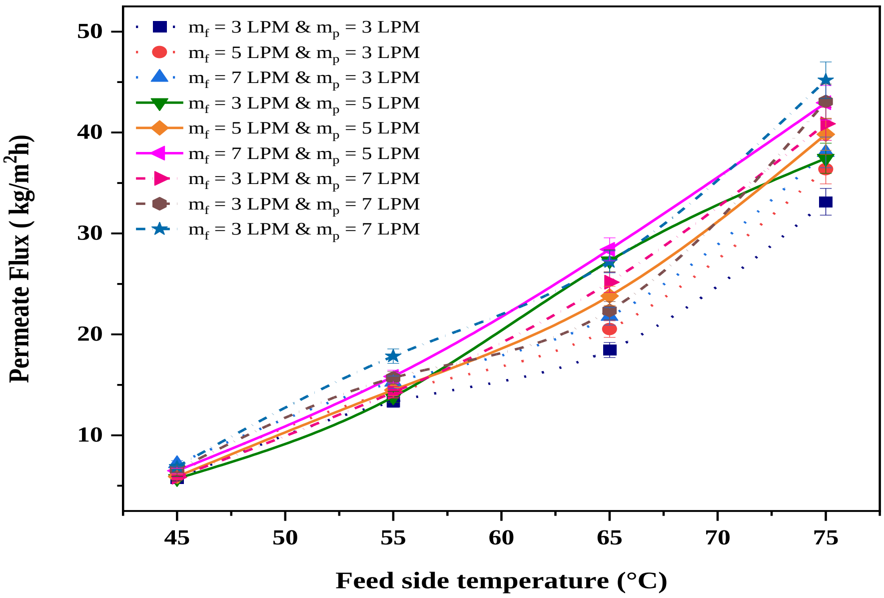

Figure 3. Permeate flux variation with varying feed temperature for different combinations of m_f and m_p.

It is worth mentioning that irrespective of the mass flow rate of the feed solution, the variation in the permeate flow was less significant at a minimum feed-side temperature of 45 °C. From Figure 3, it can be identified that the difference in permeate flux was more significant when the feed solution temperature was greater than 55 °C. Thus, a maximum difference in the permeate flux was identified for a maximum feed solution temperature of 75 °C and for varying mass flow rates of feed and permeate solutions.

A similar trend of increasing flux with an increase in the solution temperature was identified in an experimental study with a PVDF membrane by Fan et al., where a maximum flux of about 18.9 kg/m^{2}h was achieved at an operating temperature of 73 °C and 25 °C across the feed and permeate sides, respectively [34]. Therefore, the increasing trend of permeate flux with an increase in the feed flow rate can be attributed to the combined effects of temperature and concentration polarization, for all the examined feed temperatures. However, the temperature disparity between the bulk streams and membrane surfaces decreased with the heat transfer coefficient across the boundary layer due to the effect of increasing feed flow rate that contributes to a higher temperature difference between the bulk and membrane temperature on the feed side of the membrane [35]. Therefore, with an increase in the feed flow rate, the permeate flux also increased [36].

3.2. Effect of Permeate Flow Rate on Permeate Flux for Varying Feed Flow Rate/Temperature

The influence of permeate flow rates on the permeate flux is shown in Figure 4. It can be identified that the permeate flux did not vary significantly with the variation in the feed flow rates at a constant feed temperature of 45 °C. A similar trend was achieved even with the variation in the permeate flow rates in the present DCMD system equipped with a Teflon-coated PVDF membrane. This is because of the effect of the low-temperature difference maintained between feed and permeate fluids, which contributes to less vapor travel via the membrane from the feed to permeate side. It was identified that the increase in the permeate flux was significant for the condition of higher feed temperature along with higher feed and permeate flow rates. Figure 4 also depicts the variation in permeate flux for varying the feed flow rate and temperature, respectively. It can be identified that when the feed temperature was 15 °C higher than the permeate, the vapor penetration through the Teflon-coated PVDF membrane was minimum, and this phenomenon was found to be true for all the feed flow rates considered. For a temperature of about 55 °C, it is evident that the permeate flux improved by ~18% for the condition of 7 LPM permeate flow rate, compared to a lower rate of 3 LPM (Figure 4).

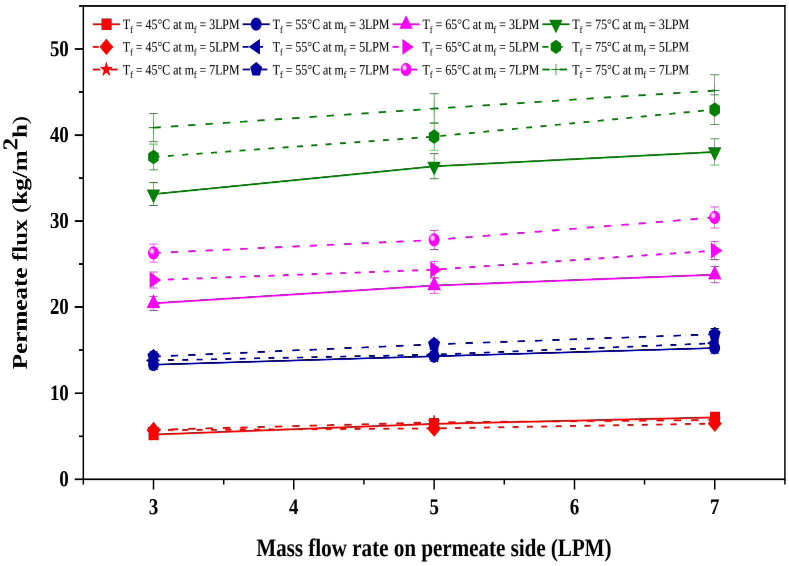

Figure 4. Variation in permeate flux with variation in feed/permeate flow rate and feed temperature.

Similarly, for the cases of higher feed temperatures of 65 °C and 75 °C, the permeate flux improvement was found to be decreasing at the rates of 15.75% and 10.57% respectively. Thus, the aforementioned results indicate that for a given permeate flow rate, the variation in the rate of permeate flux achieved with a change in the feed flow rate and temperature was a significant factor to be examined for evaluating the characteristics of a DCMD system. Therefore, for the present system with a Teflon-coated PVDF membrane, it was inferred that the permeate flux production did not vary much with the variation in the lower feed temperatures from 45 °C to 55 °C. However, the variation in permeate flux was identified to be predominant at higher feed temperatures of 65 °C and 75 °C. In the case of 65 °C, around ~28.56% of greater flux difference was achieved between the 3 and 7 LPM of permeate mass flow rate. Similarly at 75 °C, there was a ~17.62% improvement in permeate flux between the 3 and 7 LPM on the permeate side, as identified during the experimentation. Comparing the overall perspective, it can be inferred that the generation of permeate flux was higher for higher feed temperature (75 °C) and flow rate (7 LPM). This can be attributed to the higher membrane heat transfer coefficient experienced as a result of the positive variation in the flow characteristics with increasing Reynolds and Nusselt numbers, achieved with an increase in the feed flow rate [37]. Owing to the enhancement in the membrane heat transfer coefficient, the boundary layer resistance between the feed-side fluid and feed–membrane interface decreased, contributing to a nearly constant feed temperature that aids in achieving a higher temperature polarization coefficient (TPC) that contributes to augmented flux [38]. Subsequently, this played a significant role in enhancing the mass transfer across the Teflon-coated PVDF membrane. Furthermore, the increase in the temperature gradient across the membrane also enhanced the effect of vapor penetration from the feed to the permeate side [39]. Thus, it can be inferred that increasing the feed flow rate had a predominant effect of improving the permeate flux across the membrane contributing to higher freshwater productivity, compared to the influence of increasing permeate flow rate.

3.3. Effect of m_p, m_f, and Feed Temperature on Temperature Polarization Coefficient (TPC)

The temperature polarization coefficient (TPC) depends on the feed/permeate temperatures and the corresponding surface temperature across both sides of the membrane. Figure 5 depicts the variation in TPC for varying feed temperatures and feed/permeates flow rates. For a constant feed mass flow rate of 3 LPM and varying permeate mass flow rates (3, 5, and 7 LPM), the highest TPC value was achieved for a higher permeate flow rate of 7 LPM and feed temperature. Similarly, for a constant feed-side mass flow rate of 5 and 7 LPM, a higher TPC value was achieved with a 7 LPM permeate-side flow rate and higher feed temperature. It was identified that the difference in TPC value for a fixed feed temperature was significantly based on the feed flow rates. This difference was identified to decrease with the feed temperature owing to the reduction in the temperature difference between feed/permeate fluids and the surface temperatures across the corresponding sides of the membrane that increased the permeate flux of the system. The experimental highest TPC value of 0.62 was achieved when the feed flow rate was maximum at 7 LPM, irrespective of the feed temperatures. Additionally, during experimentation, it was also identified that at a constant permeate-side mass flow rate of 7 LPM, the variation in the TPC values reduced irrespective of feed flow rate (3, 5, and 7 LPM) at a higher feed temperature of 75 °C. Thus, the above results indicated that it is desirable to operate the present DCMD system at a feed flow rate of 3 LPM instead of 7 LPM as similar TPC values were achieved for all three different flow rates. This can subsequently contribute to lower energy consumptions on the pumping device (P1) due to the requirement of lower loads to achieve a similar output of permeate flux, as achieved with higher flow rates. In the case of other permeate flow rates of 3 and 5 LPM, TPC values on varying feed-side mass flow rates started to converge with increasing feed-side temperature of the bulk fluid.

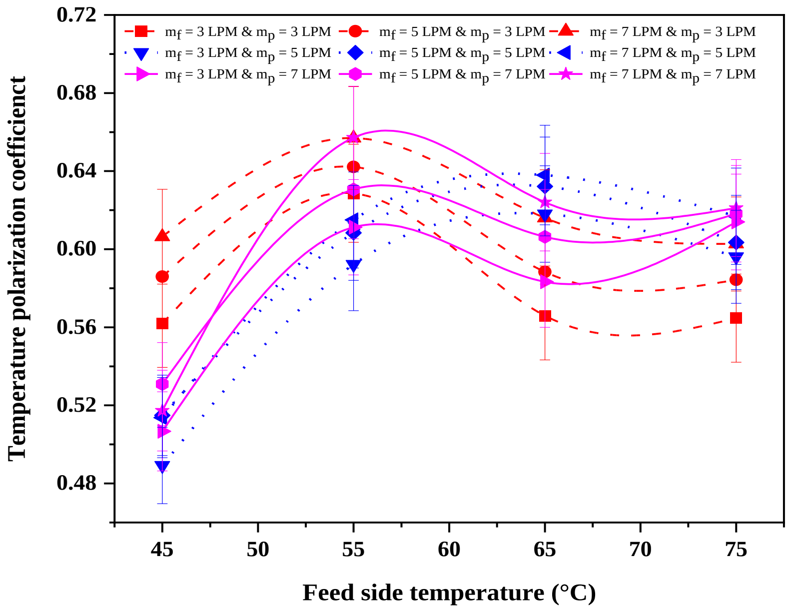

Figure 5. Characteristics of TPC with variation in feed/permeate flow rate and feed temperature.

3.4. Effect of m_p, m_f, and Feed Temperature on Evaporative Efficiency (EE)

Figure 6 depicts the variation in the evaporative efficiency (EE) of the DCMD system equipped with the Teflon-coated PVDF membrane and was determined using Equation (6). The influence of inlet feed temperature/flow rate and permeate flows rate on EE is depicted in the figure. With an increase in the feed temperature, the permeate flux also increased, contributing to improved EE [28]. Thus, a high EE of about 78.22% was identified to exist for the optimum operating conditions of feed and permeate flow rates of 7 LPM along with a feed temperature of about 75 °C. Similarly, a low evaporative efficiency of about 62.06% existed for feed and permeate solution flow rates of 3 LPM when the feed solution temperature was 45 °C. From the experimental study, it was evident that the DCMD system's performance was chiefly influenced by the feed/permeate solution temperatures and their corresponding flow rates.

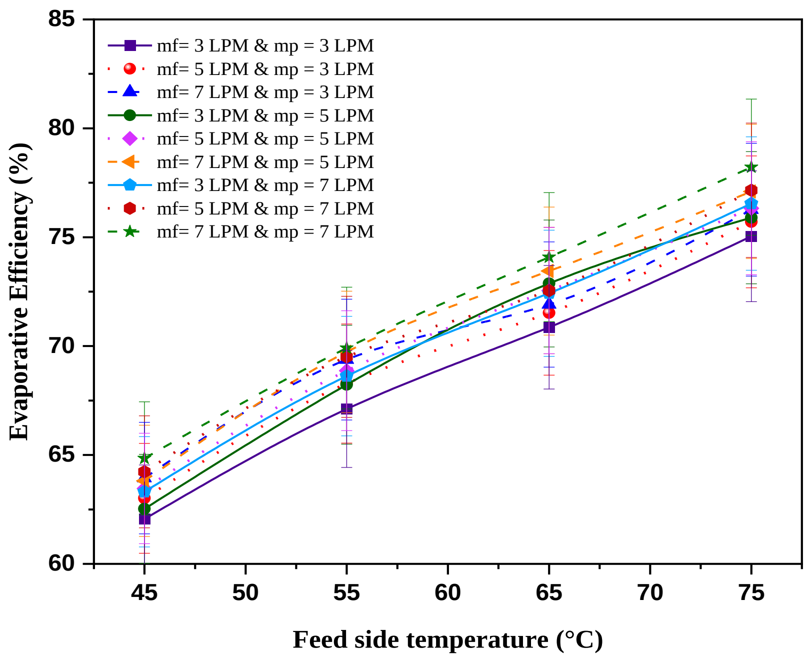

Figure 6. Variation in EE with variation in feed/permeate flow rate and feed temperature.

3.5. Comparison with Previous Literature

The performance of the present Teflon-coated PVDF membrane DCMD module was compared with the preexisting commercially available membrane technologies, as shown in Table 1. It can be identified that the addition of Teflon onto the PVDF membrane aided in achieving a higher permeate flux of 45.18 kg/m^{2}h, compared to the other similar hydrophobic membranes.

Table 1. Generation of permeate flux noted in literature.

Membrane	Porosity (%)	Thickness (µm)	Flux (kg/m^{2}h)	Reference
PTFE + PP	75	180	28	[40]
PTFE + HDPE	70	175	38	[40]
PP	70	-	29.17	[41]
PVDF	75	125	36.27	[33]
PVDF + Teflon	70	250	45.18	(Present study)

3.6. Uncertainty Analysis

To determine the errors in the experimental data, uncertainty analysis was carried out. The total uncertainty (W_T) includes both the systematic errors (owing to calibration, accuracy of the instruments, and data acquisition) and random errors. Therefore, it was estimated using the standard deviation method, which is the root-mean-square sum of the system and random errors indicated by [42]:

$$W_T = \sqrt{\sum_{i=1}^{n} E^2{}_{s,i} + \sum_{i=1}^{n} E^2{}_{r,i}} \tag{9}$$

where E_s and E_r represent the system and random errors, respectively. Further, n represents the number of error sources and $E_{r,i}$ can be calculated as [43]:

$$E_{r,i} = \sqrt{\frac{\sum_{i=1}^{n} (\varphi_i - \overline{\varphi})^2}{N(N-1)}} \tag{10}$$

where φ and N indicate the parameter's average value and the number of times it has been measured, respectively. Table 2 depicts the information on the measured quantities along with their related uncertainties.

Table 2. Uncertainty of the measured parameters.

Parameter	Instruments	Range	Accuracy	Total Uncertainty
Temperature	RTD	0–100 °C	±0.2 °C	±1.7%
Flow rate	Rotometer	0–10 LPM	±0.2 LPM	±2%

4. Cost Analysis

In addition to the experimental performance, cost analysis indicates the economic feasibility of any system. Therefore, detailed cost analysis was carried out for the present DCMD system along with evaluation of the payback period. The water production cost (WPC) was accounted for considering the major parameters that include the daily freshwater productivity (Q_w), system (or) plant availability (f), and total annual cost (AC_{total}) cost using the following equation [44]:

$$WPC = \frac{AC_{total}}{f \times Q_w \times 365} \tag{11}$$

The economic analysis was executed with the assumed values of plant availability (f), plant life (n), interest rate, amortization factor (a), specific labor cost, and brine disposal rate of 90%, 20, 5%, 0.08 per year, INR 3.87/m^3, and 0.06 kwh/m^3, respectively [44]. The results of the detailed economic analysis are summarized in Table 3, indicating a payback period of ~0.21 years.

Table 3. Economic analysis of the present system.

Particulars	Solar-Powered MD System (Cost in INR, Rupees)
Direct Capital Cost (DCC)	
Membrane cost	54,000
MD equipment	240,000
Total cost of MD Module (Membrane cost + MD equipment)	294,000
Indirect capital cost (ICC, 10% of DCC)	29,400
Capital Cost (DCC + ICC)	323,400
Annual operation and maintenance cost ($AC_{O\&M}$)	
Annual maintenance cost (AC_{MT}) (2% of AC $_{fixed}$)	
Membrane replacement cost (AC_{MR}) (20% of total cost of MD module)	58,800
Annual Labor cost (AC_{Labour})	510.84
Annual brine disposal cost (AC_{BD})	63.36
Annual electric cost ($AC_{electricity}$)	3000
$AC_{O\&M} = AC_{MR} + AC_{Labour} + AC_{BD} + AC_{electricity}$	62,885
$AC_{fixed} = a \times CC$	25,872
$AC_{total} = AC_{fixed} + AC_{O\&M}$	88,757
Q_w (m^3/day)	0.362
Water production cost	748.49/m^3
Distilled water cost	15/L [26]
Payback period	0.21 years

5. Conclusions

Based on the present experimental performance evaluation of a solar ETC-powered DCMD system equipped with a Teflon-coated PVDF membrane, the following major findings are reported:

(i) A maximum permeate flux of 45.18 kg/m^{2}h was achieved for optimum feed and permeate fluid temperatures of 75 °C and 30 °C, respectively, along with optimum flow rates of 7 LPM across both sides of the hydrophobic membrane.

(ii) A higher permeate flux was found to exist for a maximum feed flow rate of 7 LPM irrespective of the feed temperature (45–75 °C), indicating the predominant influence of the former parameter.

(iii) The difference in the TPC value for a given feed solution temperature was identified to be significant for different feed flow rates. A high TPC value of 0.62 was achieved when the feed flow rate was a maximum of 7 LPM, irrespective of the feed temperatures.

(iv) A higher evaporative efficiency of 78.22% was achieved from the present solar ETC-powered DCMD system for maximum feed/permeate flow rates of 7 LPM and a maximum feed temperature of 75 °C. Further, the system experienced a lower evaporative efficiency of 62.06% with a decrement in the fluid flow rates to 3 LPM.

Author Contributions: P.P.C.K.: conceptualization, methodology, validation, formal analysis, investigation, writing—original draft; G.K.: conceptualization, evaluation; R.A.: conceptualization, methodology, supervision, project administration, funding acquisition; R.S.: writing—review editing, investigation, supervision; R.V.: review and editing. All authors have read and agreed to the published version of the manuscript.

Funding: This research received no external funding.

Institutional Review Board Statement: Not applicable.

Informed Consent Statement: Not applicable.

Data Availability Statement: Not applicable.

Acknowledgments: The authors gratefully acknowledge the financial and instrumentation support provided by the National Institute of Ocean Technology (NIOT), Chennai, India for the present research work.

Conflicts of Interest: The authors declare no conflict of interest.

Nomenclature

Acronyms	
AC_{BD}	Annual brine disposal cost
$AC_{electricity}$	Annual electric cost
AC_{Labour}	Annual Labor cost
AC_{MR}	Membrane replacement cost
AC_{MT}	Annual maintenance cost
$AC_{O\&M}$	Annual operation and maintenance cost
CPC	Compound parabolic collector
DAQ	Data acquisition system
DCC	Direct Capital Cost
DCMD	Direct Contact Membrane Distillation
EE	Evaporative efficiency
ETSC	Evacuated Tube Solar Collector
HFP	Hexafluoropropylene
HNT	Halloysite
kW	Kilowatt
LEP	Liquid entry pressure
LPM	Liter per Minute
MD	Membrane distillation
PE	Polyethylene
PTFE	Polyfluoroethylene
PVDF	Polyvinylidene fluoride
TPC	Temperature Polarization coefficient
WPC	Water production cost
Symbols	
a	amortization factor
AC_{total}	total annual cost
B_m	mass transfer coefficient
d_p	membrane pore of size
d_{Pc}	pressure difference on cold side
d_{Ph}	pressure difference on hot side
f	plant availability
IR	Interest rate (%)
J_w	permeate flux (kg/m^{2}s)
Kn	Knudsen number
p	plant life (years)
P_{wf}	vapor pressure (Pa) across the feed side
P_{wp}	vapor pressure (Pa) across the permeate sides
Q_C	conductive heat flux (W/m^2)
Q_V	evaporative mass flux (W/m^2)
Q_w	fresh water production in m^3/day
T_{ci}	Cold-side inlet Temperature
T_{co}	cold side outlet Temperature
T_f,	bulk feed temperature
T_{hi}	hot-side Inlet temperature
T_{ho}	hot-side Outlet Temperature
T_{mf}	temperature across the feed sides
T_{mp}	temperature across the permeate sides
T_p	bulk permeate temperature
W_T	total uncertainty
ΔH	enthalpy of evaporation (kJ/kg)
Λ	mean free path

References

1. Luo, T.; Young, R.; Reig, P. *Aqueduct Projected Water Stress Country Rankings*; Technical Note; World Resources Institute: Washington, DC, USA, 2015; pp. 1–16.
2. UN World Water Development Report 2021. 2021. Available online: https://www.unwater.org/publications/un-world-water-development-report-2021/ (accessed on 21 March 2021).
3. Tiwari, A.; Rathod, M.K.; Kumar, A. A comprehensive review of solar-driven desalination systems and its advancements. *Environ. Dev. Sustain.* **2022**, 1–32. [CrossRef]
4. Mezher, T.; Fath, H.; Abbas, Z.; Khalid, A. Techno-economic assessment and environmental impacts of desalination technologies. *Desalination* **2011**, *266*, 263–273. [CrossRef]
5. Horseman, T.; Yin, Y.; Christie, K.S.; Wang, Z.; Tong, T.; Lin, S. Wetting, Scaling, and Fouling in Membrane Distillation: State-of-the-Art Insights on Fundamental Mechanisms and Mitigation Strategies. *ACS ES T Eng.* **2021**, *1*, 117–140. [CrossRef]
6. Belessiotis, V.; Kalogirou, S.; Delyannis, E. *Membrane Distillation*; Academic Press: Cambridge, MA, USA, 2016; pp. 191–251. [CrossRef]
7. Wang, P.; Chung, T.S. Recent advances in membrane distillation processes: Membrane development, configuration design and application exploring. *J. Membr. Sci.* **2015**, *474*, 39–56. [CrossRef]
8. Yan, Z.; Yang, H.; Qu, F.; Yu, H.; Liang, H.; Li, G.; Ma, J. Reverse osmosis brine treatment using direct contact membrane distillation: Effects of feed temperature and velocity. *Desalination* **2017**, *423*, 149–156. [CrossRef]
9. Khayet, M. Membranes and theoretical modeling of membrane distillation: A review. *Adv. Colloid Interface Sci.* **2011**, *164*, 56–88. [CrossRef]
10. Bodel, B.R. Distillation of Saline Water Using Silicone Rubber Membrane. U.S. Patent 3361645A, 9 August 1968.
11. Wu, Y.; Kong, Y.; Lin, X.; Liu, W.; Xu, J. Surface-modified hydrophilic membranes in membrane distillation. *J. Membr. Sci.* **1992**, *72*, 189–196. [CrossRef]
12. Kong, Y.; Lin, X.; Wu, Y.; Chen, J.; Xu, J. Plasma polymerization of octafluorocyclobutane and hydrophobic microporous composite membranes for membrane distillation. *J. Appl. Polym. Sci.* **1992**, *46*, 191–199. [CrossRef]
13. Hubadillah, S.K.; Tai, Z.S.; Othman, M.H.D.; Harun, Z.; Jamalludin, M.R.; Rahman, M.A.; Jaafar, J.; Ismail, A.F. Hydrophobic ceramic membrane for membrane distillation: A mini review on preparation, characterization, and applications. *Sep. Purif. Technol.* **2019**, *217*, 71–84. [CrossRef]
14. Lawson, K.W.; Lloyd, D.R. Membrane distillation. II. Direct contact MD. *J. Membr. Sci.* **1996**, *120*, 123–133. [CrossRef]
15. Curcio, E.; Drioli, E. Membrane Distillation and Related Operations—A Review. *Sep. Purif. Rev.* **2005**, *34*, 35–86. [CrossRef]
16. Rácz, G.; Kerker, S.; Kovács, Z.; Vatai, G.; Ebrahimi, M.; Czermak, P. Theoretical and Experimental Approaches of Liquid Entry Pressure Determination in Membrane Distillation Processes. *Period. Polytech. Chem. Eng.* **2014**, *58*, 81–91. [CrossRef]
17. Li, J.-M.; Xu, Z.-K.; Liu, Z.-M.; Yuan, W.-F.; Xiang, H.; Wang, S.-Y.; Xu, Y.-Y. Microporous polypropylene and polyethylene hollow fiber membranes. Part 3. Experimental studies on membrane distillation for desalination. *Desalination* **2003**, *155*, 153–156. [CrossRef]
18. Liu, F.; Hashim, N.A.; Liu, Y.; Abed, M.M.; Li, K. Progress in the production and modification of PVDF membranes. *J. Membr. Sci.* **2011**, *375*, 1–27. [CrossRef]
19. Ravi, J.; Othman, M.H.D.; Tai, Z.S.; El-Badawy, T.; Matsuura, T.; Kurniawan, T.A. Comparative DCMD performance of hydrophobic-hydrophilic dual-layer hollow fibre PVDF membranes incorporated with different concentrations of carbon-based nanoparticles. *Sep. Purif. Technol.* **2021**, *274*, 118948. [CrossRef]
20. AbdulKadir, W.A.F.W.; Ahmad, A.L.; Ooi, B.S. A water-repellent PVDF-HNT membrane for high and low concentrations of oxytetracycline treatment via DCMD: An experimental investigation. *Chem. Eng. J.* **2021**, *422*, 129644. [CrossRef]
21. Makanjuola, O.; Anis, S.F.; Hashaikeh, R. Enhancing DCMD vapor flux of PVDF-HFP membrane with hydrophilic silica fibers. *Sep. Purif. Technol.* **2021**, *263*, 118361. [CrossRef]
22. Twibi, M.F.; Othman, M.H.D.; Hubadillah, S.K.; Alftessi, S.A.; Adam, M.R.B.; Ismail, A.F.; Rahman, M.A.; Jaafar, J.; Raji, Y.O.; Aziz, M.H.A.; et al. Hydrophobic mullite ceramic hollow fibre membrane (Hy-MHFM) for seawater desalination via direct contact membrane distillation (DCMD). *J. Eur. Ceram. Soc.* **2021**, *41*, 6578–6585. [CrossRef]
23. Saffarini, R.B.; Summers, E.K.; Arafat, H.A.; Lienhard, J.H. Technical evaluation of stand-alone solar powered membrane distillation systems. *Desalination* **2012**, *286*, 332–341. [CrossRef]
24. El Amali, A.; Bouguecha, S.; Maalej, M. Experimental study of air gap and direct contact membrane distillation configurations: Application to geothermal and seawater desalination. *Desalination* **2004**, *168*, 357. [CrossRef]
25. Lokare, O.; Tavakkoli, S.; Wadekar, S.; Khanna, V.; Vidic, R.D. Fouling in direct contact membrane distillation of produced water from unconventional gas extraction. *J. Membr. Sci.* **2017**, *524*, 493–501. [CrossRef]
26. Pounraj, P.; Winston, D.P.; Kabeel, A.; Kumar, B.P.; Manokar, A.M.; Sathyamurthy, R.; Christabel, S.C. Experimental investigation on Peltier based hybrid PV/T active solar still for enhancing the overall performance. *Energy Convers. Manag.* **2018**, *168*, 371–381. [CrossRef]
27. Kumar, B.P.; Winston, D.P.; Pounraj, P.; Manokar, A.M.; Sathyamurthy, R.; Kabeel, A. Experimental investigation on hybrid PV/T active solar still with effective heating and cover cooling method. *Desalination* **2018**, *435*, 140–151. [CrossRef]
28. Chandrashekara, M.; Yadav, A. Water desalination system using solar heat: A review. *Renew. Sustain. Energy Rev.* **2017**, *67*, 1308–1330. [CrossRef]

29. Walton, J.; Lu, H.; Turner, C.; Solis, S.; Hein, H. Solar and Waste Heat Desalination by Membrane Distillation, Desalination and Water Purification Research and Development Program Report. Available online: https://www.usbr.gov/research/dwpr/reportpdfs/report081.pdf (accessed on 28 April 2022).
30. Hogan, P.A.; Sudjito; Fane, A.G.; Morrison, G.L. Desalination by solar heated membrane distillation. *Desalination* **1991**, *81*, 81–90. [CrossRef]
31. Yang, X.; Wang, R.; Shi, L.; Fane, A.G.; Debowski, M. Performance improvement of PVDF hollow fiber-based membrane distillation process. *J. Membr. Sci.* **2011**, *369*, 437–447. [CrossRef]
32. Gao, L.; Zhang, J.; Gray, S.; Li, J.-D. Experimental study of hollow fiber permeate gap membrane distillation and its performance comparison with DCMD and SGMD. *Sep. Purif. Technol.* **2017**, *188*, 11–23. [CrossRef]
33. Srisurichan, S.; Jiraratananon, R.; Fane, A. Mass transfer mechanisms and transport resistances in direct contact membrane distillation process. *J. Membr. Sci.* **2006**, *277*, 186–194. [CrossRef]
34. Fan, H.; Peng, Y. Application of PVDF membranes in desalination and comparison of the VMD and DCMD processes. *Chem. Eng. Sci.* **2012**, *79*, 94–102. [CrossRef]
35. Phattaranawik, J.; Jiraratananon, R.; Fane, A.G. Heat transport and membrane distillation coefficients in direct contact membrane distillation. *J. Membr. Sci.* **2003**, *212*, 177–193. [CrossRef]
36. Hou, D.; Wang, J.; Zhao, C.; Wang, B.; Luan, Z.; Sun, X. Fluoride removal from brackish groundwater by direct contact membrane distillation. *J. Environ. Sci.* **2010**, *22*, 1860–1867. [CrossRef]
37. Mengual, J.; Khayet, M.; Godino, M. Heat and mass transfer in vacuum membrane distillation. *Int. J. Heat Mass Transf.* **2004**, *47*, 865–875. [CrossRef]
38. Alsaery, S. Development of Highly Porous Flat Sheet Polyvinylidene Fluoride (PVDF) Membranes for Membrane Distillation. Master's Thesis, King Abdullah University of Sciences and Technology, Thuwal, Saudi Arabia, 2017.
39. Alkhudhiri, A.; Darwish, N.; Hilal, N. Membrane distillation: A comprehensive review. *Desalination* **2012**, *287*, 2–18. [CrossRef]
40. Shirazi, M.M.A.; Kargari, A.; Tabatabaei, M. Evaluation of commercial PTFE membranes in desalination by direct contact membrane distillation. *Chem. Eng. Process. Process Intensif.* **2014**, *76*, 16–25. [CrossRef]
41. Gryta, M.; Tomaszewska, M. Heat transport in the membrane distillation process. *J. Membr. Sci.* **1998**, *144*, 211–222. [CrossRef]
42. Shafieian, A.; Khiadani, M.; Nosrati, A. Performance analysis of a thermal-driven tubular direct contact membrane distillation system. *Appl. Therm. Eng.* **2019**, *159*, 113887. [CrossRef]
43. Shafieian, A.; Osman, J.J.; Khiadani, M.; Nosrati, A. Enhancing heat pipe solar water heating systems performance using a novel variable mass flow rate technique and different solar working fluids. *Sol. Energy* **2019**, *186*, 191–203. [CrossRef]
44. Soomro, M.I.; Kim, W.-S.; Kim, Y.-D. Performance and cost comparison of different concentrated solar power plants integrated with direct-contact membrane distillation system. *Energy Convers. Manag.* **2020**, *221*, 113193. [CrossRef]